

Functionalized magnetic-fluorescent hybrid nanoparticles for cell labelling

Lei Lou,^a Ke Yu,^{*a} Zhengli Zhang,^a Bo Li,^a Jianzhong Zhu,^a Yiting Wang,^b Rong Huang^a and Ziqiang Zhu^a

Received 18th January 2011, Accepted 16th March 2011

DOI: 10.1039/c1nr10066a

A facile method of synthesizing 60 nm magnetic-fluorescent core-shell bifunctional nanocomposites with the ability to label cells is presented. Hydrophobic trioctylphosphine oxide (TOPO)-capped CdSe@ZnS quantum dots (QDs) were assembled on polyethyleneimine (PEI)-coated Fe₃O₄ nanoparticles (MNP). Polyethyleneimine was utilized for the realization of multifunction, including attaching 4 nm TOPO capped CdSe@ZnS quantum dots onto magnetite particles, altering the surface properties of quantum dots from hydrophobic to hydrophilic as well as preventing the formation of large aggregates. Results show that these water-soluble hybrid nanocomposites exhibit good colloidal stability and retain good magnetic and fluorescent properties. Because TOPO-capped QDs are assembled instead of their water-soluble equivalents, the nanocomposites are still highly luminescent with no shift in the PL peak position and present long-term fluorescence stability. Moreover, TAT peptide (GRKKRRQRRPQ) functionalized hybrid nanoparticles were also studied due to their combined magnetic enrichment and optical detection for cell separation and rapid cell labelling. A cell viability assay revealed good biocompatibility of these hybrid nanoparticles. The potential application of the new magnetic-fluorescent nanocomposites in biological and medicine is demonstrated.

1. Introduction

In recent years, increasing efforts have been devoted to the design and fabrication of nanostructured functional materials. Research on these materials has revealed an exciting trend of transforming them from single functional to double functional, and even multifunctional. Among these multifunctional nanocomposites, magnetic and fluorescent inorganic nanoparticles have attracted considerable attention due to their small size, homogeneous structures, convenience in chemical modification and broad range of potential applications.^{1,2}

Quantum dots (QDs) as fluorescent probes remained attractive over the last decades owing to their size-dependent fluorescent properties and potential applications in biological and medical areas. These fluorescent semiconductor (*e.g.* II–VI) nanocrystals have strong characteristic spectral emission, which can be tuned to a desired energy level by altering particle size, size distribution and composition of the nanocrystals. Instead of single core quantum dots, the method of growing a shell of a few atomic layers of a material with a larger band gap on top of the nanocrystal core (*i.e.* CdSe@ZnS core-shell QDs) is used more and more extensively to sufficiently improve the luminescence quantum efficiency and to protect surface atoms from oxidation and other chemical reactions.^{3–5} With increasing understanding

of the accompanying photophysics, lots of applications have been developed by controlling particle morphology, such as cell labelling, cell migration tracking and *in vivo* imaging.^{6–8}

On the other hand, magnetic nanoparticles have also attracted much attention due to their remarkable magnetic properties, nontoxic nature, and ease of synthesis, which lead to their successful applications in biotechnology and medicine.⁹ They can also be used as contrast agents in magnetic resonance imaging.^{10–13} Another unique feature of magnetic nanoparticles is their significant response to magnetic field, which opens the possibilities to many applications by magnetic control, including biological separation, protein purification, bacteria detection, and drug delivery.^{14–19} Therefore, the application field of magnetic nanoparticles is expanding at high speed.

Magnetic-fluorescent nanocomposite materials, which combine both magnetic and fluorescent properties in one entity, have been studied extensively, particularly in those of potential applications in biotechnology and medicine. There are several types of magnetic-fluorescent nanocomposites reported before, including polymer-coated magnetic cores treated with fluorescent entities,²⁰ magnetic core coated with silica shell containing fluorescent components,^{21,22} magnetic-fluorescent heterodimer nanoparticles²³ and magnetic core directly coated with a semi-conducting shell.²⁴ All these nanostructures have both advantages and disadvantages. For example, Rosenzweig and co-workers²⁰ reported a thiol coupling approach to synthesize nanocomposites consisting of polymer coated γ -Fe₂O₃ superparamagnetic cores and CdSe/ZnS quantum dots shell. But it was still a challenge to couple these hydrophobic QDs to the

^aKey Laboratory of Polar Materials and Devices (Ministry of Education of China), Department of Electronic Engineering, East China Normal University, Shanghai, 200241, China. E-mail: yk5188@263.net

^bInstitutes for Advanced Interdisciplinary Research, East China Normal University, Shanghai, 200062, China

hydrophilic magnetic beads, and the magnetic properties of these nanocomposites had not been investigated. Successful synthesis of a water-soluble hybrid material consisting of quantum dots and magnetic nanoparticles (MPs) encapsulated in a silica shell was reported by Ying and co-workers.²¹ In their work, the dimension of nanocomposites was well controlled, in which silica provided an effective barrier against aggregation. However, the reaction period was still long, and the quantum yield (QY) was not quite satisfying. Generally, for most magnetic fluorescent nanocomposites, the challenges lie in the complicated approach during synthesis, hard control of magnetic aggregation, low magnetic or fluorescent intensity, *etc.*

To evaluate the biological contribution as well as the potential toxicity of the magnetic-fluorescent nanocomposites in biology and medicine, lots of efforts have been devoted to the *in vivo* and *in vitro* toxicity analysis. As previously reported, magnetic-fluorescent nanocomposites were usually functionalized on surface to improve biocompatibility and reduce nonspecific binding, such as coating with amphiphilic polymers,²⁵ conjugation with polypeptide,²⁶ coupling with antibodies,²⁷ modification with vitamin,²⁸ *etc.* In this work, TAT peptide was adopted to give the magnetic-fluorescent composites a desired bioactivity and reduced cytotoxicity. An MTT assay was also utilized to reveal the low toxicity of the hybrid nanoparticles.

In this paper, we report the simple and fast synthesis of Fe₃O₄-PEI-QDs nanocomposites with good magnetic and fluorescent properties remaining. The 50 nm Fe₃O₄ nanospheres were prepared with the cationic polyethyleneimine (PEI) self-assembled on the surface, which has the multifunction of attaching 4 nm trioctylphosphine oxide (TOPO) capped CdSe@ZnS quantum dots onto magnetite particles, altering the surface properties of quantum dots from hydrophobic to hydrophilic as well as avoiding the formation of large aggregates. At last, water-soluble TAT peptide (GRKKRRQRRRPQ) functionalized hybrid nanoparticles were derived from these magnetic-fluorescent nanocomposites, which were finally used for cell imaging. An external magnetic field was used to separate the labelled cells, which were successfully imaged using a fluorescence microscope, utilizing the fluorescence property of hybrid nanoparticles.

2. Materials and methods

2.1 Materials

Polyethyleneimine (PEI, branched, $M_w \sim 25000$) and Hexamethyldisilathiane ((TMS)₂S) were obtained from Sigma–Aldrich. Trioctylphosphine oxide (TOPO, 90% pure) and trioctylphosphine (TOP, 95% pure) were obtained from Strem and Fluka, respectively. Dimethylcadmium (CdMe₂) and diethylzinc (ZnEt₂) were purchased from Alfa and Fluka, respectively. TAT peptide with terminal cysteine group with 95% purity was purchased from GenScript. The other regular reagents were purchased from Shanghai Chemical Reagent (China). All of the chemicals were the highest purity available or analytical grade. All the chemicals were at analytical grade or the highest purity level.

2.2 Synthesis of CdSe@ZnS quantum dots

ZnS capped CdSe quantum dots were prepared in a two-step process as previously reported with minor change:⁴ Firstly, CdSe

core particles were synthesised, precipitated and washed. Subsequently, these cores were redispersed into a coordinating solvent and the ZnS shell was added.

CdSe quantum dots were synthesized *via* the pyrolysis of the organometallic precursors, dimethylcadmium and trioctylphosphine selenide, in a coordinating solvent, trioctylphosphine oxide (TOPO) as described previously.²⁹ The TOPO was heated to 340 °C, degassed and aerated with nitrogen, and then injected with organometallic precursors. The initially formed cores were grown at 290 °C. Anhydrous methanol and anhydrous 1-butanol were used to isolate, purify and precipitate the TOPO capped CdSe nanocrystallites size-selectively, and then the precipitated powder was redispersed in hexane. 5 g of TOPO was heated to 190 °C in vacuum for several hours and then cooled down to 60 °C, followed by adding 0.5 mL trioctylphosphine (TOP). The fresh prepared CdSe dots in hexane were then transferred into the reaction vessel by a syringe.

These CdSe nanocrystals were passivated with the following procedure: Equimolar amounts of the Zn and S precursors, diethylzinc (ZnEt₂) and hexamethyldisilathiane ((TMS)₂S) were dissolved in TOP. The precursor solution was injected to the reaction flask using a syringe, which contained CdSe dots dispersed in TOPO and TOP at a constant temperature of 200 °C under an atmosphere of N₂. The Zn and S precursors were added dropwisely to the reaction mixture which is being vigorously stirred. After then, the mixture was cooled down to 90 °C and stirred for several hours. Subsequently, 5 mL dry butanol were added and the reaction mixture was stirred for another several hours at 60 °C. The flask was allowed to cool down to room temperature, and the nanoparticles were stored in the growth solution to keep the passivation of TOPO. The final nanoparticles were precipitated with dry methanol, redispersed in chloroform and used for the subsequent experiments.

2.3 Synthesis of PEI capped Fe₃O₄ nanoparticles

The magnetic Fe₃O₄ nanoparticles were prepared by coprecipitating of Fe²⁺ and Fe³⁺ ions (in the molar ratio of 1:2) by alkaline solution and hydrothermal treating.³⁰ Milli-Q water was re-deionized and deoxygenated by bubbling with N₂ gas for 1 h prior to use. Mixture of FeCl₂·4H₂O (0.1 M) and FeCl₃·6H₂O (0.2 M) was prepared as a source of iron by dissolving the respective chemicals in water under vigorous stirring. Then NaOH solution (1 M) was added dropwisely under continuous stirring at 300 rpm. The precipitate was heated at 90 °C for 2 h in the presence of PEI solution, during which PEI self-assembled on the Fe₃O₄ nanoparticles (Fig. 1b). The pH was maintained at a constant value during the reaction process. The whole reaction can be described by the following reaction scheme:



Particles were magnetically separated from the reaction mixture by placing a neodymium magnet below the reaction vessel. It took 10 min to capture all magnetic particles before disposing of the reaction solution. The collected Fe₃O₄-PEI particles were rinsed for 5 times with Milli-Q water and finally formed a suspension of Fe₃O₄.

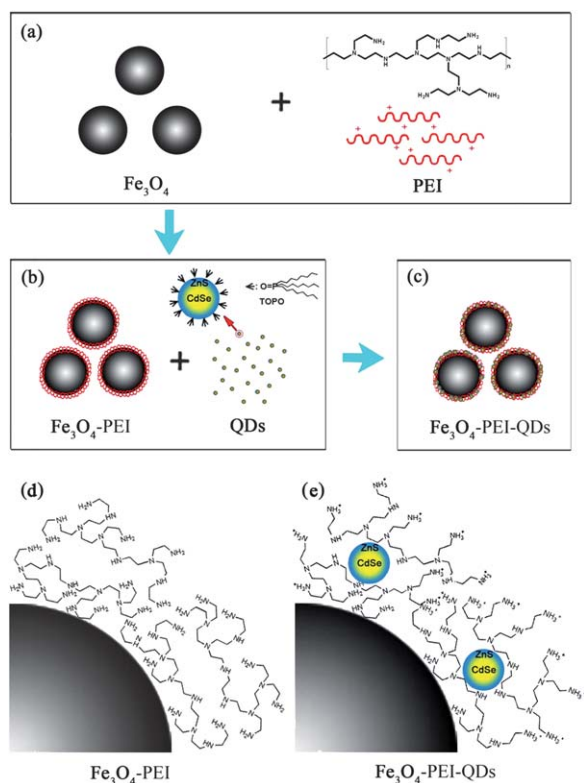


Fig. 1 Schematic representation of the synthesis of QDs-magnetite core-shell particles: (a) Self-assembly of cationic polyethyleneimine (PEI) onto negatively charged magnetite (Fe₃O₄). (b) Mixing of Fe₃O₄-PEI with quantum dots to obtain MNP-PEI-QDs nanocomposites. (c) MNP-PEI-QDs nanocomposites. (d)~(e) Schematic representation of switching of quantum dots from lipophilic to hydrophilic.

2.4 Preparation of the fluorescent magnetic nanocomposites

20 μ L (60 μ g) of PEI coated magnetic nanospheres were precipitated by a neodymium disk magnet. The sample was washed with 1 mL of water, 4 \times 1 mL of methanol and 1 mL of chloroform, and then suspended in 1 mL of chloroform which contained excess of fresh-prepared quantum dots (20 μ L). The mixture solution was rotated for 1 h at room temperature. After the reaction, the nanocomposites were magnetically precipitated and then washed with 1 mL of chloroform, 4 \times 1 mL of methanol and 1 mL of water, and finally redispersed in Milli-Q water.

2.5 TAT peptide functionalization of hybrid nanoparticles

TAT peptide functionalization was performed using an earlier protocol.³¹ 2 mL of fresh-prepared MNP-PEI-QDs solution was diluted with borate buffer (pH 9.5) and mixed with SMCC solution (1 mg dissolved in 1 mL of dimethylformamide) and finally incubated for 1 h. Then the nanoparticles were separated from free reagents by means of Na₂HPO₄-induced precipitation. The precipitated particles were separated from free reagents, dissolved in fresh phosphate buffer, and then mixed with 100 μ L of TAT peptide solutions (2 mg of TAT peptide dissolved in 1 mL of phosphate buffer solution) and incubated at 4 $^{\circ}$ C overnight. Finally, the particles were purified from free peptide by overnight dialysis against deionized water, using a membrane

of 12–14 kDa MWCO. The solution of peptide-conjugated hybrid nanoparticles was diluted with Tris buffer (pH 7.0) and stored at 4 $^{\circ}$ C.

2.6 Cell labelling

Human lung cancer cells, NCI-H460 cells grown in tissue culture flask were subcultured in 24-well tissue culture plates using 0.5 mL of culture medium in each plate, followed by incubation with 10–100 μ L of MNP-PEI-QDs solution for 15 min and 1 h at room temperature, respectively. The cells were separated from the suspension using a permanent magnet and washed with PBS buffer and cell culture media to purify cells from free nanoparticles.

2.7 Toxicity assay

In order to test the toxicity of the magnetic fluorescent nanocomposites, MTT (3-(4,5-dimethylthiazol-2-yl)-2,5-diphenyltetrazolium bromide) assay kit (Invitrogen, Singapore) was adopted here. According to the typical procedure, cells were seeded in a 24-well plate for 24 h, and then incubated with different concentrations of hybrid nanoparticles functionalized with TAT peptide in 5% CO₂ at 37 $^{\circ}$ C. Cells were then washed three times followed by addition of 10 mL MTT solution to each well and incubated for 2 h at 37 $^{\circ}$ C. Then 100 μ L of SDS-HCl (sodium dodecyl sulfate-HCl) solution was added to each well and was then mixed thoroughly. Finally the absorbance of the resulting solution was measured at 570 nm using a microplate reader.

2.8 Characterization

The morphology and structure of the products were characterized by transmission electron microscopy (TEM, Jeol JEM-2100) and X-ray diffraction (XRD, D/MAX 2550V) with Cu K α radiation. Particle size distributions were obtained based on dynamic light scattering (DLS) principles with a Brookhaven 90 Plus particle sizer. UV–visible absorption spectra were obtained by a Cary 100 UV–vis spectrophotometer. Photoluminescence (PL) spectra were recorded on a Hitachi F-4500 Fluorescent spectrophotometer. Magnetization loops were measured at room temperature using a physical property measurement system (PPMS, Quantum Design). Digital fluorescence microscopy images were taken from the Inverted biological microscope (Olympus).

3. Results and discussion

3.1 Attachment of QDs on Fe₃O₄

The schematic representation of the synthesis of MNP-PEI-QDs is shown as Fig. 1a–1c. At first, cationic polyethyleneimine (PEI) was self-assembled onto negatively charged magnetite nanoparticles (Fe₃O₄). After then Fe₃O₄-PEI nanospheres were mixed with TOPO capped CdSe@ZnS quantum dots to obtain MNP-PEI-QDs nanocomposites and the QDs were covalently bonded to the PEI layer. After the reaction, the MNP-PEI-QDs nanocomposites were deposited by a neodymium magnet and washed

with chloroform to wipe off the redundant quantum dots. Finally the nanocomposites were redispersed in water.

Although the CdSe@ZnS core-shell structure offers good quantum yield (79%), altering the QD surface properties from hydrophobic to hydrophilic is still an essential step for functionalizing QDs for biological applications due to the aqueous nature of the biological environment. In order to get rid of this drawback, it is necessary to alter the surface properties of quantum dots from hydrophobic to hydrophilic, which can be realized with the help of amphiphilic hyperbranched polyethyleneimine (PEI).³² In previous work, Nann³² has shown that highly luminescent water-soluble QDs can be prepared by adding PEI to TOPO-capped QDs in chloroform,³² and Mulvaney³³ and colleagues have shown that when the microspheres coated with PEI are shaken along with TOPO-capped QDs in chloroform, the QDs can be transferred from the organic phase to microspheres in the aqueous phase. In addition to aggregation resistance, the positively charged PEI layer plays an important role in transferring the quantum dots surface properties from hydrophobic to hydrophilic when quantum dots are attached. The hypothetical mechanism of the amphiphilic phase-transfer is depicted in Fig. 1d–1e. It is reported in other paper that the amphiphilic and polycation characters of PEI can help to displace the original surface ligands (TOPO) and build a very stable colloid with QDs in chloroform. After being extracted from chloroform, the solvents were deprotonated by the PEI since the pH-value is strongly basic in water and PEI is positively charged.³²

3.2 Synthesis of TOPO capped CdSe@ZnS core-shell nanocrystals

The CdSe@ZnS core-shell structure has attracted lots of attention over years. In addition to higher photoluminescence quantum yields, ZnS overcoated particles are more robust than organically passivated CdSe dots. As is indicated in Fig. 2a, the monodispersed TOPO capped CdSe@ZnS core-shell nanocrystals with average size of about 4 nm were prepared as reported before. The high-resolution TEM image (Fig. 2a) shows well-resolved lattice fringes, which are continuous throughout the entire particle. Well-defined interfaces between CdSe core and ZnS shell cannot be observed in any of the samples, and the growth of the ZnS shell appears to be epitaxial.

3.3 Synthesis of PEI capped magnetic nanoparticles

The magnetic nanospheres with about 50nm diameter were prepared by a simple, cheap and harmless hydrothermal method using Fe²⁺ and Fe³⁺ ions (in the molar ratio of 1:2) under basic condition. An important step during the synthesis is the addition of the polycation, PEI, onto the surface of Fe₃O₄ nanospheres. The immobilization of PEI layer during the synthesis of Fe₃O₄ nanoparticles was found to be an effective method of controlling the aggregation of magnetic nanoparticles. The positively charged PEI was attached to the negatively charged MNP effectively and formed a stable polyelectrolyte layer *via* electrostatic self-assembly by adding PEI during the synthesis procedures. As is known to all, Fe₃O₄ nanoparticles are easy to aggregate due to their magnetic feature, nevertheless, the as-prepared nanoparticles shown in the TEM image (Fig. 2b) exhibits nearly spherical morphology with good dispersity and have an average diameter of 50 nm. A 1~2 nm polyelectrolyte

layer can be clearly identified by the HRTEM (Fig. 2c), which also exhibits the ordered lattice feature and without staking faults, indicating the highly crystallinity of the nanoparticles. The d-spacing of 0.48 nm can be indexed to the d-value of (1 1 1) plane of Fe₃O₄. As previously reported, the growth axis of [1 1 1] is common for Fe₃O₄ nanoparticles. Selected area electron diffraction (SAED) was performed on isolated crystals of the Fe₃O₄ (Inset of Fig. 2c). The lattice parameters obtained were consistent with that of a single crystal of Fe₃O₄.

3.4 Structure of MNP-PEI-QDs

The TEM image in Fig. 2d shows hybrid nanoparticles of an average size of 60nm with a spread of QDs attached. A closer HRTEM image of a single particle is demonstrated in Fig. 2e, which clearly indicates the uniform capping of 4 nm QDs on the surface of Fe₃O₄ nanospheres. According to TEM image analysis, the number of QDs attached on each PEI-coated Fe₃O₄ is estimated to be 120. Fig. 2f reveals the difference in lattice fringes between the QDs (indicated with arrows) and Fe₃O₄ cores, which provides strong evidence to the composite nature of the particle. To prove the growth of CdSe@ZnS shell, Energy Dispersive Spectrometer (EDS) was used to indicate the existence of iron, oxygen, cadmium, selenium, zinc and sulfur (Fig. 2g). The carbon peak results from the sample grid. The relatively high zinc and sulfur peaks of QDs could also indicate the presence of multiple layers of ZnS on the surface of the CdSe QDs. The X-ray diffraction (XRD) pattern of the nanocomposites (Fig. 2h) also indicates the existence of both CdSe@ZnS and Fe₃O₄. The pattern can be suitably indexed on a wurtzite structure of ZnS (▼), CdSe (◆) and cubic Fe₃O₄. All diffraction peaks of Fe₃O₄ can be perfectly indexed to face centered cubic magnetite with lattice constant $a = 8.393 \text{ \AA}$ (JPCD 82-1533). No peaks for other impurities were detected in the spectrum, revealing the high purity of the products was pretty high. The evolutional of the XRD pattern during the growth of the QDs shows a wurtzite structure of CdSe (JPCD 77-2307) and ZnS (JPCD 36-1450) on the magnetic nanoparticles. The additional broadness of the XRD reflections in the composite-structure pattern results from the very small domain size characteristic of the polycrystalline Fe₃O₄ and CdSe and ZnS crystal.

Dynamic light scattering (DLS) measurements of the hydrodynamic (effective) diameters of the particles were used to study particle aggregation behavior. Fe₃O₄ and MNP-PEI-QDs nanoparticles were dispersed in a 10 mM NaCl background electrolyte at pH 7 to simulate a biological environment for up to 1 h after sonication treatment. The size distribution histograms of Fe₃O₄ and MNP-PEI-QDs are shown in Fig. 3a and Fig.3b respectively. The size of the nanoparticles mainly ranges from 40 nm to 60 nm and the average diameter is about 48.9 nm, while the size of MNP-PEI-QDs nanocomposites mainly ranges from 50 nm to 65 nm with an average diameter of 57.8 nm, which both agree well with the TEM images.

3.5 Magnetic properties of MNP-PEI-QDs

Since the Fe₃O₄ nanoparticles are mainly used to manipulate synthesized particles under an applied magnetic field, it is important to characterize the magnetic properties of the hybrid

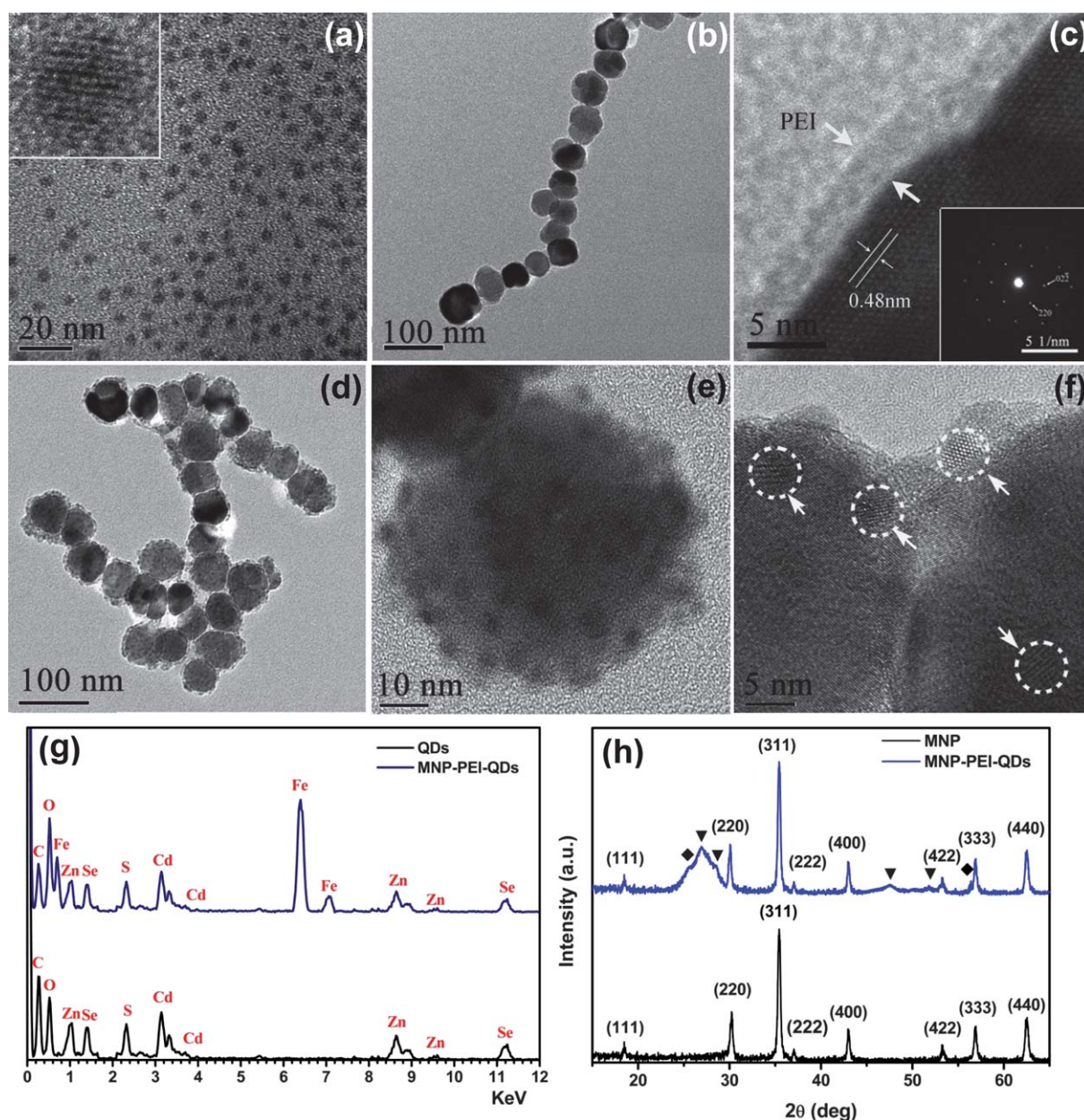


Fig. 2 (a) TEM image of CdSe@ZnS quantum dots, the inset is the HRTEM image of a single nanosphere; (b) TEM image of Fe₃O₄-PEI nanoparticles; (c) HRTEM image of the edge of Fe₃O₄-PEI nanoparticles, arrows indicating a thin layer of PEI; The inset is SAED of the Fe₃O₄-PEI nanoparticle; (d) TEM image of MNP-PEI-QDs nanocomposites; (e) HRTEM image of a single MNP-PEI-QDs nanosphere; (f) HRTEM image of MNP-PEI-QDs nanosphere, with arrows indicating the quantum dots; (g) EDS pattern of CdSe@ZnS quantum dots and MNP-PEI-QDs nanocomposites; (h) XRD pattern of Fe₃O₄ nanocrystal and MNP-PEI-QDs nanocomposites. ZnS (▼), CdSe (◆) and cubic Fe₃O₄ of wurtzite structure were indexed.

nanoparticles. The magnetic properties were measured on both Fe₃O₄ nanoparticles and MNP-PEI-QDs nanocomposites to reveal the effect of the coating of quantum dots at both 5 K and room temperature. These data were presented in electromagnetic units per gram of solid sample. As indicated in Fig. 4a, at room temperature, both samples showed no hysteresis, *i.e.* no remanence or coercivity, which is consistent with paramagnetic behavior of Fe₃O₄. It can also be seen that the particles are ferromagnetic at 5 K, with a coercivity of 300 Oe (Fig. 4b). At both 5K and room temperature, the saturation magnetization (σ_s) of MNP-PEI-QDs nanocomposites shows a decrease of 85% compared with Fe₃O₄. The decrease in magnetism is mainly

attributed to the presence of QDs on particles, which is an unavoidable consequence of QDs loading, indicating that the overcoating has weakened the magnetization to a certain extent, yet the nanocomposites still remained paramagnetic.

When under an external field, the suspension could be separated by a neodymium magnet in 5 min (Fig. 6c). The MNP-PEI-QDs nanocomposites were attracted to one side of the vial as the arrows indicate, showing that the particles maintain strong magnetism even after QDs coating. When the magnet was removed, the particles can redisperse easily into the water again. Due to the absence of any hysteresis and zero coercivity, the nanoparticles coated with QDs are easy to redisperse when the

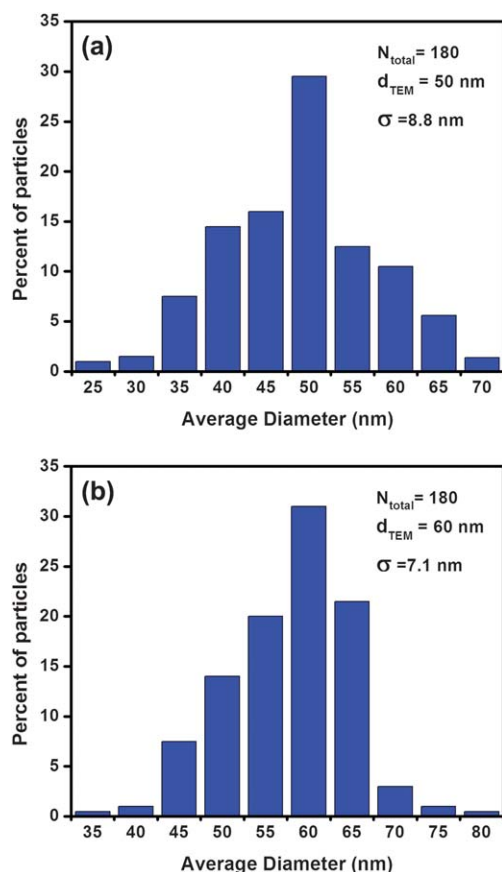


Fig. 3 (a) Particle size distribution of MNP-PEI nanoparticles deduced from dynamic light scattering (DLS); (b) Particle size distribution of MNP-PEI-QDs nanoparticles deduced from dynamic light scattering (DLS).

applied magnetic field is removed. It is critical for the magnetic luminescent nanocomposites to act as labels for separation or bioassay, which will be demonstrated later in this paper. If the particle possessed a remnant magnetic field, each individual particle would act as a small dipole magnet, resulting in aggregations and precipitation of the particles.

3.6 Fluorescent properties of MNP-PEI-QDs

The optical properties of the samples were investigated using the PL spectra and UV-vis absorption. The emission from the nanocomposites could be easily detected when excited by a UV lamp. The adsorption spectra of the CdSe@ZnS quantum dots and MNP-PEI-QDs are shown in Fig. 5a, where the absorbance peak of MNP-PEI-QDs at about 578 nm was in agreement with the maximum absorption peak of QDs, indicating the CdSe@ZnS quantum dots were attached to the Fe₃O₄ nanoparticles successfully. Fig. 5b shows PL spectra of QDs and MNP-PEI-QDs nanocomposites with no shift in the PL peak position at 592 nm, demonstrating that the quantum dots suffered little damage during the synthesis process. This feature offers a great potential to the easy synthesis of various fluorescent nanocomposites by simply altering the size of the quantum dots.

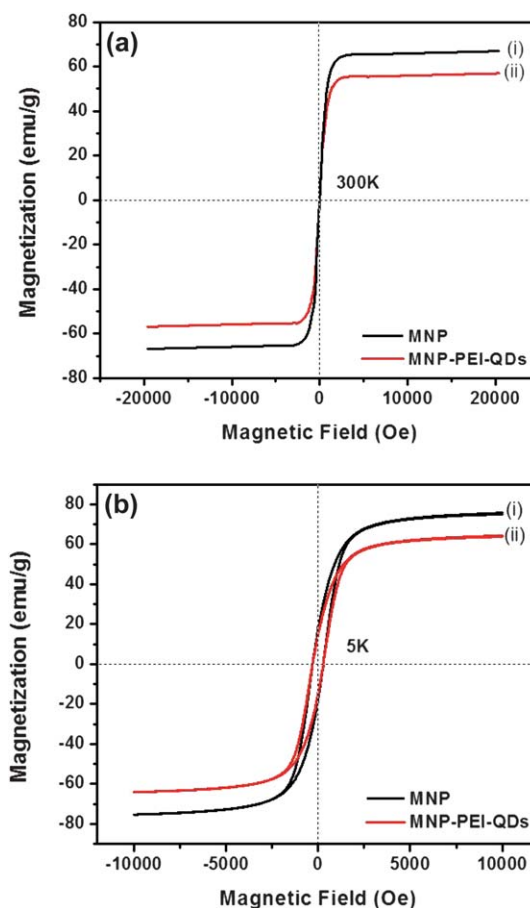


Fig. 4 (a) Magnetic hysteresis curves of (i) Fe₃O₄-PEI; (ii) MNP-PEI-QDs at room temperature. There was no hysteresis, *i.e.*, no remanence or coercivity, which is consistent with paramagnetic behaviour. (a) Magnetic hysteresis curves of (i) Fe₃O₄-PEI; (ii) MNP-PEI-QDs at 5 K with a coercivity of 300 Oe.

Photoluminescence quantum yield values (*QY*) were measured relative to the organic dye Rhodamine B in ethanol solution (*QY*. 0.95 in ethanol) using according to the following equation:³⁴

$$QY_X = QY_S * [I_X/I_S] * [A_S/A_X] * [n_X/n_S]^2 \quad (2)$$

In the equation, I_X (sample) and I_S (standard) are the integrated emission peak areas, A_X (sample) and A_S (standard) are the absorbances at the excitation wavelength, and n_X (sample) and n_S (standard) are the refractive indices of the solvents.

The optical properties of MNP-PEI-QDs exhibit no major changes after being transferred into water. The fluorescence quantum yield (*QY*) of the fresh prepared quantum dots is about 79%, while the *QY* of MNP-PEI-QDs is about 40% of the original value. The decrease of *QY* is a common phenomenon because quantum yield is highly sensitive to the surface of the QDs, especially with respect to ligand chemistry. Herein the original hydrophobic capping ligands of TOPO capped QDs were displaced by hydrophilic ones.

In addition, the fluorescence stability of the magnetic-fluorescent nanocomposites was studied as an important factor. As is

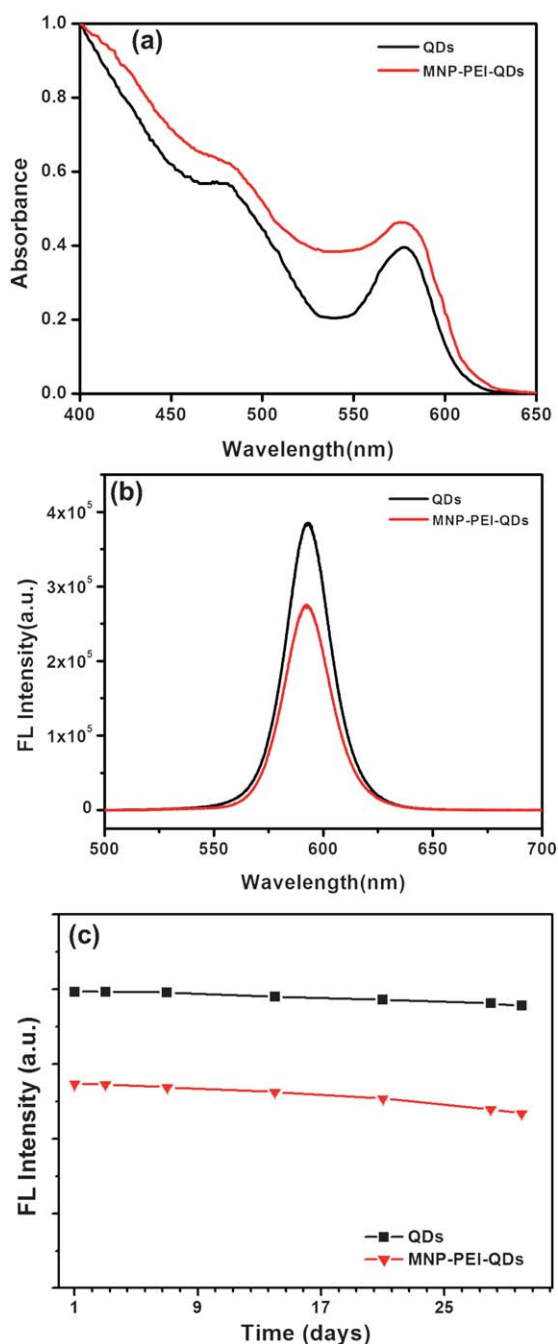


Fig. 5 Optical properties of magnetic-fluorescent hybrid nanoparticles (a) UV-vis adsorption spectra of QDs (black) and MNP-PEI-QDs (red) nanocomposites; (b) absorbance-calibrated photoluminescence spectra of QDs (black) and MNP-PEI-QDs (red) nanocomposites; (c) fluorescence stability of QDs (black) and MNP-PEI-QDs (red) nanocomposites.

indicated in Fig. 5c, the fluorescence intensity of quantum dots remained good during one month's measurements. For magnetic-fluorescent nanoparticles, although the fluorescent stability is not as good as quantum dots, the fluorescent intensity of the hybrid nanoparticles also remained strong after one month's storage.

The photos of QDs and MNP-PEI-QDs solution were taken under daylight and ultraviolet with the excitation wavelength of 366 nm (Fig. 6a–f). The quantum dots showed bright fluorescence under the UV excitation as usual (Fig. 6d). MNP-PEI-QDs

suspension showed brown color under daylight (Fig. 6b), while orange color under UV excitation (Fig. 6e), which agreed well with the fluorescent properties of the nanocomposites. In Fig. 6f, because of the magnetic moments of Fe_3O_4 , the magnet attracted the fluorescent MNP-PEI-QDs nanoparticles completely to the side of the vial in 5 min, as is indicated by the arrows, and there was only a clear solution remained.

3.7 Cell labeling

As a preliminary investigation of the performance of MNP-PEI-QDs for biological applications, the as-prepared nanoparticles were applied to label cells in culture. The cell labelling was studied using the human lung cancer cells, NCI-H460. TAT peptide functionalization is achieved by using N-succinimidyl 4-(maleimidomethyl)cyclohexanecarboxylate (SMCC) as conjugation reagent.³¹ Due to the low nanoparticles uptake under 4 °C, all uptake experiments were conducted at 37 °C. The cells were incubated with the nanoparticles for 15 min and 1 h respectively. To demonstrate the separation capability of the hybrid nanoparticles, an external magnetic field was used to separate the labelled cells, and the purified cells were washed for several times to remove free particles. Further digital fluorescence microscopy was performed to observe the cells. The binding activity of hybrid nanoparticles to the cells is shown in Fig. 7a. It can be observed that lots of cancer cells were separated from the suspension using a permanent magnet and labelling is restricted to the cell surface after the unbound hybrid nanoparticles were removed. Orange fluorescence was emitted from the cells surface, which remained almost the same color as QDs. When these cells were maintained at 37 °C for 1 h, the labelling effect was predominant in the perinuclear region (Fig. 7b), and there were still some residual hybrid nanoparticles on the

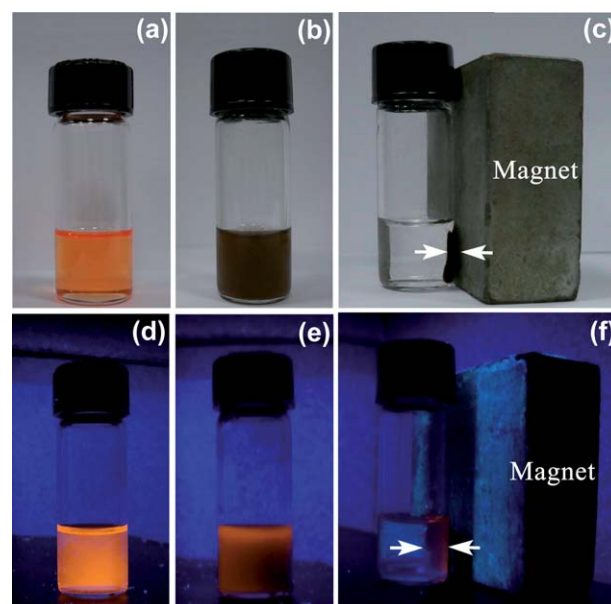


Fig. 6 Pictures of (a) CdSe@ZnS quantum dots; (b) MNP-PEI-QDs aqueous solution; (c) MNP-PEI-QDs aqueous solution under the magnetic field under daylight; (d)–(f) shows the corresponding pictures under UV excitation ($\lambda_{\text{exc}} = 366 \text{ nm}$).

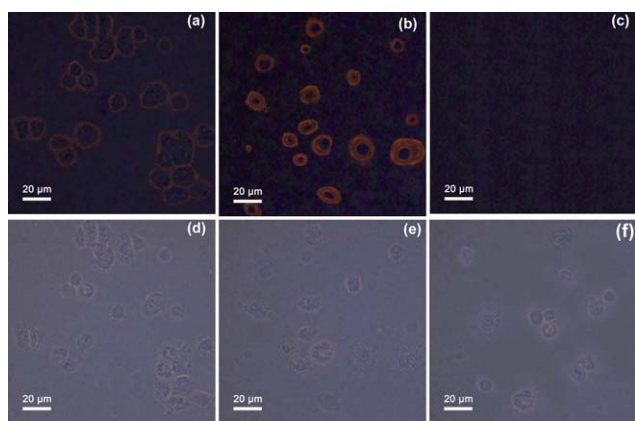


Fig. 7 (a) Fluorescence image of human lung cancer cells, NCI-H460 cells after labelling with TAT peptide-functionalized MNP-PEI-QDs nanoparticles for 15 minutes; Labelling is restricted to the cell surface. (b) Fluorescence image of NCI-H460 cells after labelling hybrid nanoparticles for 1 hour; Labelling is predominantly perinuclear. (c) Fluorescence image of NCI-H460 cells after labelling with MNP-PEI-QDs nanoparticles without TAT peptide-functionalized for 1 hour. (d)~(f) are the corresponding images in bright field.

membrane. In contrast, the cells were imaged under the same condition in a control experiment where they were incubated with MNP-PEI-QDs nanocomposites without TAT peptide functionalization (Fig. 7c). No specific binding was found in the control experiment. This suggests that the hybrid nanoparticles were internalized by endocytosis instead of being bounded on the plasma membranes. It indicates that cells constitutively utilized the method of endocytosing the cell surface proteins, which, in turn, suggests that QD labelling may not have any deleterious effects on normal endocytic physiology.

3.8 Cytotoxicity

Biocompatibility is a critical issue for nanomaterials' biological applications since lots of nanomaterials have strong cytotoxicity.

To verify the biocompatibility of these hybrid magnetic fluorescent nanoparticles, cell viability upon exposure to TAT

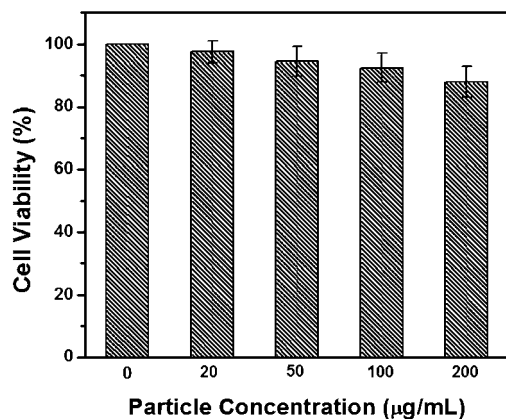


Fig. 8 Viability of NCI-H460 cells after incubation with different concentrations of hybrid nanoparticles as measured by MTT assay. The error bars represent the fluctuations among four independent measurements.

peptide functionalized hybrid nanoparticles was measured by an MTT (3-(4,5-dimethylthiazol-2-yl)-2,5-diphenyltetrazolium bromide) assay. Fig. 8 shows the concentration effect of the hybrid nanoparticles on cell viability after incubation. The results clearly indicate that the cell viability remains as high as 88% even at a high concentration of nanoparticles ($200 \mu\text{g mL}^{-1}$). Thus, the low toxicity of the particles toward cells demonstrated the potential application of the MNP-PEI-QDs in biological and medicine.

4. Conclusions

In conclusion, we report a facile method for synthesizing 60nm magnetic-fluorescent core-shell bifunctional nanocomposites with the ability to label cells. Briefly, we successfully synthesized the water-soluble MNP-PEI-QDs nanocomposites by assembling hydrophobic trioctylphosphine oxide (TOPO)-capped CdSe@ZnS quantum dots (QDs) on polyethyleneimine (PEI)-coated Fe₃O₄ nanoparticles (MNP). The multifunction of polyethyleneimine is discussed by attaching 4 nm TOPO capped CdSe@ZnS quantum dots onto magnetite particles, altering the surface properties of quantum dots from hydrophobic to hydrophilic and preventing the formation of large aggregates. These water-soluble hybrid nanocomposites retain the magnetic property of Fe₃O₄ with still high luminescence and good fluorescence stability with no shift in the PL peak position, which consists well with the pictures taken under UV-lamp. Finally, the excellent fluorescence and magnetism properties of TAT peptide functionalized hybrid nanoparticles offer a combined magnetic enrichment and optical detection strategy for cancer cells detection, which also displayed very low toxicity to cells even at high concentrations.

Acknowledgements

The authors acknowledge the financial support from the NSF of China (Grant Nos 60976014, 60976004 and 11074075), the Key Basic Research Project of Scientific and Technology Committee of Shanghai (Grant No. 09DJ1400200), the Specialized Research Fund for the Doctoral Program of Higher Education (Grant No. 20070269016), and PCSIRT.

Notes and references

- 1 J. H. Gao, B. Zhang, Y. Gao, Y. Pan, X. X. Zhang and B. Xu, *J. Am. Chem. Soc.*, 2007, **129**, 11928.
- 2 H. Kim, M. Achermann, L. P. Balet, J. A. Hollingsworth and V. I. Klimov, *J. Am. Chem. Soc.*, 2005, **127**, 544–546.
- 3 X. Peng, M. C. Schlamp, A. Kadavanich and A. P. Alivisatos, *J. Am. Chem. Soc.*, 1997, **119**, 7019.
- 4 M. A. Hines and P. Guyot-Sionnest, *J. Phys. Chem.*, 1996, **100**, 468.
- 5 A. R. Kortan, R. Hull, R. L. Opila, M. G. Bawendi, M. L. Steigerwald, P. J. Carroll and L. E. Brus, *J. Am. Chem. Soc.*, 1990, **112**, 1327.
- 6 M. Bruchez Jr., M. Moronne, P. Gin, S. Weiss and A. P. Alivisatos, *Science*, 1998, **281**, 2013.
- 7 W. C. W. Chan, D. J. Maxwell, X. H. Gao, R. E. Bailey, M. Y. Han and S. M. Nie, *Curr. Opin. Biotechnol.*, 2002, **13**, 40.
- 8 X. Michalet, F. F. Pinaud, L. A. Bentolila, J. M. Tsay, S. Doose, J. J. Li, G. Sundaresan, A. M. Wu, S. S. Gambhir and S. Weiss, *Science*, 2005, **307**, 538–544.
- 9 U. Schwertmann and R. M. Cornell, *Iron Oxides in the Laboratory: Preparation and Characterization*, 2nd ed; Wiley-VCH: Weinheim, Germany, 2000.

- 10 I. J. de Vries, W. J. Lesterhuis, J. O. Barentsz, P. Verdijk, J. H. van Krieken, O. C. Boerman, W. J. Oyen, J. J. Bonenkamp, J. B. Boezeman, G. J. Adema, J. W. Bulte, T. W. Scheenen, C. J. Punt, A. Heerschap and C. G. Figdor, *Nat. Biotechnol.*, 2005, **23**, 1407–1413.
- 11 H. Lee, E. Lee, D. K. Kim, N. K. Jang, Y. Y. Jeong and S. Jon, *J. Am. Chem. Soc.*, 2006, **128**, 7383–7389.
- 12 J. H. Lee, Y. W. Jun, S. I. Yeon, J. S. Shin and J. Cheon, *Angew. Chem., Int. Ed.*, 2006, **45**, 8160.
- 13 W. J. Rieter, K. M. L. Taylor, H. An, W. Lin and W. Lin, *J. Am. Chem. Soc.*, 2006, **128**, 9024–9025.
- 14 H. W. Gu, P. L. Ho, K. W. T. Tsang, L. Wang and B. Xu, *J. Am. Chem. Soc.*, 2003, **125**, 15702.
- 15 I. S. Lee, N. Lee, J. Park, B. H. Kim, Y. W. Yi, T. Kim, T. K. Kim, I. H. Lee, S. R. Paik and T. Hyeon, *J. Am. Chem. Soc.*, 2006, **128**, 10658.
- 16 J. H. Gao, L. Li, P. L. Ho, G. C. Mak, H. W. Gu and B. Xu, *Adv. Mater.*, 2006, **18**, 3145–3148.
- 17 S. Giri, B. G. Trewyn, M. P. Stellmaker and V. S. Y. Lin, *Angew. Chem., Int. Ed.*, 2005, **44**, 5038–5044.
- 18 H. Yang and Y. N. Xia, *Adv. Mater.*, 2007, **19**, 3085.
- 19 C. Wilhelm, C. Billotey, J. Roger, J. N. Pons, J. C. Bacri and F. Gazeau, *Biomaterials*, 2003, **24**, 1001–1011.
- 20 D. Wang, J. He, N. Rosenzweig and Z. Rosenzweig, *Nano Lett.*, 2004, **4**, 409–413.
- 21 D. K. Yi, S. T. Selvan, S. S. Lee, G. C. Papaefthymiou, D. Kundaliya and J. Y. Ying, *J. Am. Chem. Soc.*, 2005, **14**, 4990–4991.
- 22 T. R. Sathe, A. Agrawal and S. Nie, *Anal. Chem.*, 2006, **78**, 5627–5632.
- 23 H. W. Gu, R. K. Zheng, X. X. Zhang and B. Xu, *J. Am. Chem. Soc.*, 2004, **126**, 5664.
- 24 Q. T. Zhi, L. Z. Zhi, J. H. Gao, B. H. Huang, H. Y. Xie, M. Xie, H. D. Abrun and D. W. Pang, *Chem. Commun.*, 2009, 4025–4027.
- 25 T. R. Sathe, A. Agrawal and S. M. Nie, *Anal. Chem.*, 2006, **78**, 5627–5632.
- 26 M. Q. Chu, X. Song, D. Cheng, S. P. Liu and J. Zhu, *Nanotechnology*, 2006, **17**, 3268–3273.
- 27 G. P. Wang, E. Q. Song, H. Y. Xie, Z. L. Zhang, Z. Q. Tian, C. Zuo, D. W. Pang, D. C. Wu and Y. B. Shi, *Chem. Commun.*, 2005, 4276–4278.
- 28 H. Y. Xie, C. Zuo, Y. Liu, Z. L. Zhang, D. W. Pang, X. L. Li, J. P. Gong, C. Dickinson and W. Z. Zhou, *Small*, 2005, **1**, 506–509.
- 29 C. B. Murray, D. J. Norris and M. G. Bawendi, *J. Am. Chem. Soc.*, 1993, **115**, 8706.
- 30 P. Berger, N. B. Adelman, K. J. Beckman, D. J. Campbell, A. B. Ellis and G. C. Lisensky, *J. Chem. Educ.*, 1999, **76**, 943.
- 31 Y. Wei, N. R. Jana, S. Tan and J. Y. Ying, *Bioconjugate Chem.*, 2009, **20**, 1752.
- 32 T. Nann, *Chem. Commun.*, 2005, **13**, 1735–1736.
- 33 D. E. Gómez, I. Pastoriza-Santos and P. Mulvaney, *Small*, 2005, **1**, 238–241.
- 34 J. N. Demasa and G. A. Crosby, *J. Phys. Chem.*, 1971, **75**, 991–1024.